

# Evaluation of Imprint and Multi-Level Dynamics in Ferroelectric Capacitors

Sara Vecchi, Francesco Maria Puglisi,\* Pascal Appelt, Roberto Guido, Xuetao Wang, Stefan Slesazek, Thomas Mikolajick, and Suzanne Lancaster


Fluorite-structured ferroelectrics are one of the most promising material systems for emerging memory technologies. However, when integrated into electronic devices, these materials exhibit strong imprint effects that can lead to a failure during writing or retention operations. To improve the performance and reliability of these devices, it is cardinal to understand the physical mechanisms underlying the imprint during operation. In this work, the comparison of First-Order Reversal Curves measurements with a new gradual switching experimental approach named “Unipolar Reversal Curves” is used to analyze both the fluid imprint and the time-dependent imprint effects within a 10 nm-thick  $\text{Hf}_{0.5}\text{Zr}_{0.5}\text{O}_2$  capacitor. Interestingly, the application of delay times (ranging from 100  $\mu\text{s}$  up to 10 s) between the partial switching pulses of a Unipolar Reversal Curve sequence enables analysis of the connection between the two aforementioned imprint types. Based on these results, the study finally reports a unified physical interpretation of imprint in the context of a charge injection model, which explains both types of imprint and sheds light on the dynamics of multi-level polarization switching in ferroelectrics.

## 1. Introduction

Fluorite-structured ferroelectric thin films are one of the most promising material systems for emerging memory technologies which could lead to overcome the scaling challenges that conventional semiconductor memory and storage technologies are facing below the 22 nm node. Ferroelectric doped hafnia films allow a Complementary Metal-Oxide Semiconductor (CMOS) compatible 3D deposition via the well-established Atomic Layer Deposition (ALD) technique,<sup>[1]</sup> thickness scalability even below 10 nm,<sup>[2–5]</sup> and resilience against electrical breakdown thanks to their large bandgap (>5 eV).<sup>[6]</sup> However, these FE films suffer from several performance instabilities that still hinder their success in the marketplace.<sup>[5,7–10]</sup> Therefore, in the last decade, many research efforts have been made to identify the physical reasons behind reliability concerns arising during operating conditions, such as insufficient

switching endurance,<sup>[11,12]</sup> which are caused by fatigue or breakdown,<sup>[8,13]</sup> as well as imprint. In the case of doped ferroelectric hafnium oxide, the existence of strong imprint effects<sup>[10,14]</sup> during device operation may be crucial to understand the dominant reliability issues. In fact, also widely investigated in perovskite films,<sup>[15–19]</sup> imprint is one of the most critical degradation effects in ferroelectric thin films,<sup>[20]</sup> since it can cause an increase in operating voltage, introduction of a new and more severe retention constrain often referred to as “opposite state” (OS) retention, and in the extreme case even write failure in ferroelectric devices.<sup>[10,14,21]</sup> In literature, two main imprint phenomena are discussed, both a fluid<sup>[9]</sup> imprint and a time-dependent<sup>[22]</sup> imprint. Time-dependent imprint manifests itself as the shift of the polarization hysteresis loop along the voltage axis with time in devices set to a specific polarization state. The effect results from the generation of the internal electric field within the ferroelectric.<sup>[22]</sup> The origin of the time-dependent imprint phenomenon is currently under debate and several hypothesis have been proposed, such as generation of an oxygen vacancy profile within the ferroelectric film,<sup>[23]</sup> and/or charge injection from the electrodes in the layer at the interface with the ferroelectric.<sup>[24]</sup> On the other hand, the fluid imprint refers to a

S. Vecchi  
MDCO Italy – Applied Materials  
Via M. Ruini 74/L, Reggio Emilia (RE) 42124, Italy  
F. M. Puglisi  
Dipartimento di Ingegneria “Enzo Ferrari” – Università degli Studi di Modena e Reggio Emilia  
Via P. Vivarelli 10/1, Modena (MO) 41125, Italy  
E-mail: francescomaria.puglisi@unimore.it  
P. Appelt, R. Guido, X. Wang, S. Slesazek, T. Mikolajick, S. Lancaster  
NaMLab GmbH  
Nöthnitzer Str. 64a 01187, Dresden Germany  
T. Mikolajick  
Chair of Nanoelectronics  
TU Dresden  
Nöthnitzer Str. 64 01187, Dresden Germany

 The ORCID identification number(s) for the author(s) of this article can be found under <https://doi.org/10.1002/aelm.202400204>

© 2024 The Author(s). Advanced Electronic Materials published by Wiley-VCH GmbH. This is an open access article under the terms of the [Creative Commons Attribution](#) License, which permits use, distribution and reproduction in any medium, provided the original work is properly cited.

DOI: 10.1002/aelm.202400204

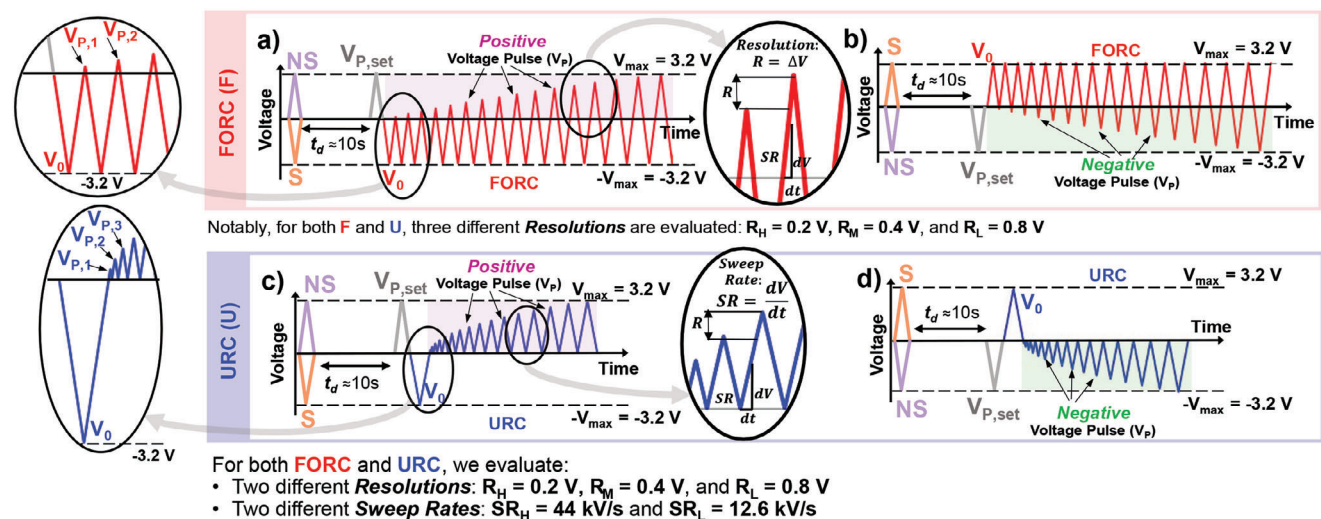


**Figure 1.** Representation of FORC train pulse for a) positive and b) negative applied bias. Here, each  $V_p$  starts from the opposite polarization state, i.e.,  $-3.2 \text{ V}$  for positive and  $+3.2 \text{ V}$  for negative polarity. URC measurements for positive c) and negative d) polarity. In URC measurements, each voltage pulse  $V_p$  starts from  $0 \text{ V}$ , independently on the polarity.

more dynamic imprint effect that strongly depends on the characteristics of the switching pulse applied and may even facilitate the continuation of domain switching. While time-dependent imprint can be associated with the charge injection at the electrode-ferroelectric interface layer and/or the redistribution of oxygen vacancies within the ferroelectric, the root cause of fluid imprint is mainly related to the charge injection into and migration across the (non-ferroelectric) interfacial layer.<sup>[9]</sup> In this work, we present new electrical measurements that allow us to probe deeper into both time-dependent and fluid imprint effects that occur in  $\text{Hf}_{0.5}\text{Zr}_{0.5}\text{O}_2$ -based ferroelectric capacitors (FeCAPs) during partial polarization switching, thereby also providing insights into the multi-level switching dynamics in such devices.

The possibility of partial switching leading to multi-level states in FeCAPs and other ferroelectric-based devices is of high interest for brain-inspired computing architectures,<sup>[25]</sup> where a multi-level device can act as a synapse and accumulate an electrical signal over multiple voltage pulses.<sup>[26]</sup> For applications requiring the processing of sensory data (e.g., image or voice recognition), brain-inspired technologies offer the possibility of vastly outperforming CMOS technologies in terms of energy consumption and fault tolerance.<sup>[27]</sup> Depending on the neural network design, different pulse timing schemes may be relevant for the weight update of ferroelectric devices<sup>[28]</sup> and ideally devices for synaptic operations could leverage different timescales to mimic short- and long-term brain plasticity.<sup>[29]</sup> It is interesting, therefore, to consider the impact of imprint, which is known to act on different timescales,<sup>[9]</sup> on multi-level device operation.

The outcomes of this study can be key to explain the microscopic mechanisms behind imprint effects arising during multi-level switching of ferroelectric  $\text{HfO}_2$  thin films, thus improving the performance and reliability of hafnia-based ferroelectric memory devices. In addition, we illustrate a unified physical interpretation of imprint, consistent with recent imprint models reported in the literature, which can explain both the time dependence and the impact of the switching history of the device.

## 2. Results and Discussion

In this study, imprint effects have been investigated in a  $10 \text{ nm}$ -thick ferroelectric  $\text{Hf}_{0.5}\text{Zr}_{0.5}\text{O}_2$ , deposited via ALD, and sandwiched between two TiAlN electrodes.<sup>[30]</sup> Local electrical breakdown of the ferroelectric layer is used to give access to the common bottom electrode, and the voltage signals are applied to the top electrode. The imprint phenomena were evaluated on fully woken-up FeCAPs. The details of the device lifetime and wake-up effects are discussed in the Supporting information (Figure S1, Supporting Information).

### 2.1. Fluid Imprint

The fluid imprint effect was investigated by using two different pulse train sequences, which are presented in Figure 1. Here, the first electrical measurement (red, upper row) refers to the First-Order Reversal Curves (FORC), i.e., a well-known test method related to the Preisach switching density,<sup>[31]</sup> which allows detailed analysis of the switching field density within the ferroelectric as a function of the electric field.<sup>[32]</sup> As depicted in detail in Figure 1, FORC measurement results are evaluated for both positive (Figure 1a) and negative (Figure 1b) applied bias (herein referred to as *polarity*). For a given voltage polarity, the FORC measurement consists in applying triangular pulses of increasing voltage magnitude until a maximum (i.e.,  $|V_{max}| = 3.2 \text{ V}$ ) is reached. Notably, in FORC measurements each voltage pulse ( $V_p$ ) starts from the maximum opposite voltage, namely  $-V_{max}$  for the positive (Figure 1a) and  $+V_{max}$  for the negative (Figure 1b) case. Therefore, by applying a given  $V_p$ , all domains with coercive fields between  $0 \text{ V}$  and the actual  $V_p$  are switched. For instance, the domains switched by applying  $V_{p,2}$  have coercive fields between  $0 \text{ V}$  and  $V_{p,2}$ , while after applying  $V_{p,6}$  all the domains with coercive fields between  $0 \text{ V}$  and  $V_{p,6}$  are switched. Naturally, since  $V_{p,2} < V_{p,6}$ , the number of domains switched by applying  $V_{p,6}$  is higher compared to the ones switched with  $V_{p,2}$ .

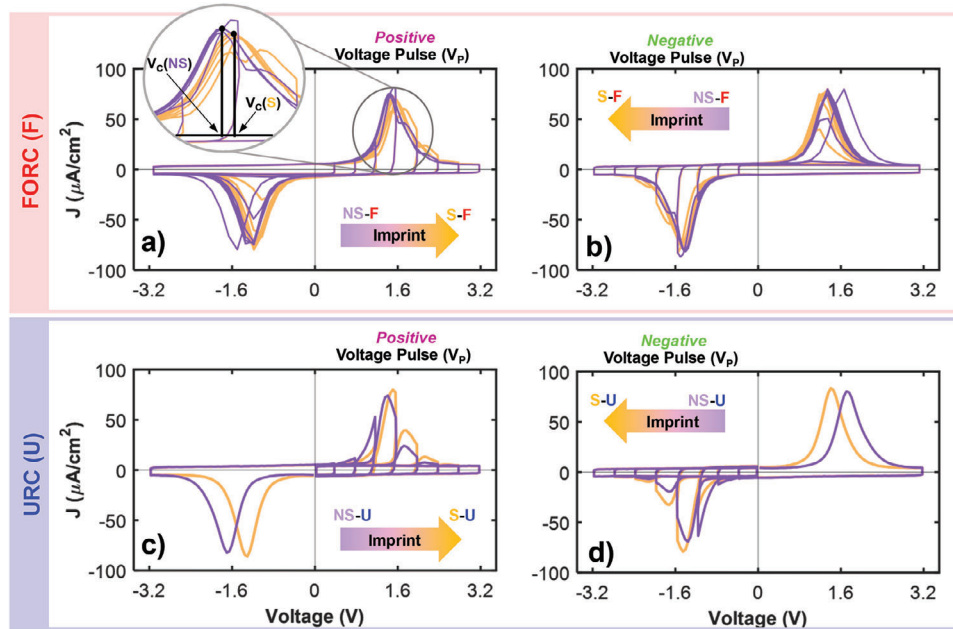


**Figure 2.** Current density ( $J$ ) versus Applied Voltage plots from FORC (a,b) and URC (c,d) measurements. Evaluation of the impact of initial device state on FORC measurements, for the a) positive and b) negative polarity. Evaluation of the impact of initial device state on URC measurements, for a) positive and b) negative polarity. To better depict the differences between the S and NS measurements, these measurement outputs refer to  $VR_M = 0.4$  V.

In the bottom row (blue) of Figure 1, we illustrate (for both polarities, i.e., Figure 1c – positive, and Figure 1d – negative) a second novel measurement routine, namely the Unipolar Reversal Curve (URC). Different from the FORC measurement in which the  $V_p$  pulses are always preceded by a  $-V_{max}$  ( $+V_{max}$ ) pulse for positive (negative) bias, during the URC measurement each  $V_p$  pulse starts from 0 V. Hence, the polarization is gradually switched without switching back in between pulses. Independent of the polarities, if we focus on the URC measurement curves (Figure 1c,d), the domains switched during a given voltage pulse, for example the third voltage pulse  $V_{p,3}$  (Figure 1c), must possess coercive voltages higher than the previous pulse (i.e.,  $V_{p,2}$ ) and smaller than or equal to the current pulse peak value (i.e.,  $V_{p,3}$  in this example). On the contrary, as highlighted previously, if we apply (for instance) the same  $V_{p,3}$  pulse in a FORC measurement (Figure 1a,b), all the domains with coercive voltages between 0 V and  $V_{p,3}$  are switched, since before such a voltage pulse the whole ferroelectric polarization was reset using the  $-V_{max}$  pulse. Hence, by influencing the switching history of the ferroelectric film differently, FORC and URC measurements complement each other. Comparing these two measurement techniques can bring new insights for evaluating the fluid imprint effects.

As depicted in Figure 1a, for both FORC and URC tests, we evaluate three different voltage resolutions (VR). Here VR describes the voltage difference between two subsequent  $V_p$  pulses. Specifically, we analyzed  $VR_H = 0.2$  V (high VR),  $VR_M = 0.4$  V (medium VR), and  $VR_L = 0.8$  V (low VR). In addition, as defined in Figure 1c, for both FORC and URC, we repeat the measurements using two different sweep rates (SR), namely  $SR_H = 44$   $\text{kV s}^{-1}$  (High SR) and  $SR_L = 12.6$   $\text{kV s}^{-1}$  (Low SR), to rule out the presence of possible RC delay effects. For sake of simplicity, in

the text we show the results related to one single sweep rate (i.e.,  $SR_L = 12.6$   $\text{kV s}^{-1}$ ), but all the trends observed and discussed here are the same for the case of  $SR_H = 44$   $\text{kV s}^{-1}$ . Likewise, even if the same behavior is verified for  $VR_M$  (i.e., 0.4 V) and  $VR_L$  (i.e., 0.8 V) resolutions, we mainly show results related to the  $VR_H$  (i.e., 0.2 V).

As shown in Figure 1, before beginning each measurement, a bipolar preset pulse sequence is applied. This consists of an initial set pulse ( $V_{p,set}$ ) and full switching pulse ( $V_0$ ) which ensure that all ferroelectric domains are switched into the same initial polarization state. We first evaluate whether pre-polarizing the ferroelectric domains in one direction or the opposite may impact the measurement result. To investigate this aspect, we set the device into an initial polarization state, roughly 10 s before applying the measurement pulse train. This initial state determines whether  $V_{p,set}$  leads to polarization switching (here labeled “S”) or not (here labelled “NS”). We apply an initial voltage pulse (i.e., S or NS), wait 10 s, and then apply  $V_{p,set}$ ,  $V_0$ , followed by the FORC/URC sequence, obtaining NS-F/NS-U and S-F/S-U. For the sake of clarity, sketches of such train pulses are illustrated in Figure 2a (FORC) and Figure 2c (URC). With that in mind, in Figure 2 we evaluate the impact of S and NS pulses by comparing, for both polarities, NS-F with S-F (Figure 2a,b) and NS-U with S-U (Figure 2c,d).

As depicted here, independent of the polarity (i.e., positive and negative) and measurement type (i.e., FORC and URC), an imprint effect emerges when an S pulse is applied 10 s before measuring, which shifts both the preset pulse and the subsequent FORC/URC measurements along the voltage axis in a direction consistent with time-dependent imprint.<sup>[33]</sup> This rigid shift in coercive voltage ( $V_c$ , see sketch in Figure 2a) is one manifestation of the time-dependent imprint effect, whereby domains switched

into one polarization orientation become more difficult to switch into the opposite direction with an increasing delay time.<sup>[22,33]</sup>

We now compare FORC to URC by keeping the same initial polarization conditions. Precisely, we want to evaluate the differences in terms of transient switching current between FORC and URC pulse sequences, therefore we compare NS-F with NS-U and S-F with S-U, separately. However, we cannot simply compare the polarization switching on each pulse between FORC and URC. Instead, it is necessary to consider that in URC measurements, pulse-by-pulse, switch only an additional portion of domains, since previously switched domains do not contribute to the current response. Therefore, as illustrated in detail in **Figure 3a**, for each  $V_p$  we compare the “effective” FORC polarization, i.e.,  $P_{EFF}^F(V_p)$ , with the URC polarization, namely  $P^U(V_p)$ . Notably, the first electrical pulse is the same for both measurements (i.e.,  $V_{p,1}$ ), therefore the integral of the charge over time is the same for the first voltage pulse. Mathematically, for  $V_{p,i}$  with  $i = 2, \dots, n$ , where  $n =$  number of  $V_p$ ,  $P_{EFF,i}^F(V_{p,i})$  is the polarization switched after applying a pulse  $V_{p,i}$  minus the polarization switched with the previous pulse, namely:

$$P_{EFF,i}^F(V_{p,i}) = P^F(V_{p,i}) - P^F(V_{p,i-1}) \quad (1)$$

With that in mind, we can compare  $P_{EFF,i}^F(V_{p,i})$  with  $P^U(V_{p,i})$  for each  $V_{p,i}$  ( $i = 2, \dots, n$ ). A comparison between the effective FORC and URC switching is reported in **Figure 3b** (S case) and **Figure 3c** (NS case). Here, it can be noted that, in all cases, the ferroelectric switching happens with lower coercive voltages with URC pulsing compared to FORC pulsing. In **Figure 3d,e**, the difference in polarization switched in the URC and the FORC measurement,  $\Delta P_{EFF}$ , is plotted, given by:

$$\Delta P_{EFF} = P^U(V_{p,j}) - P_{EFF,i}^F(V_{p,i}) \quad (2)$$

At voltages below  $|1.6 \text{ V}|$ ,  $\Delta P_{EFF}$  is positive, indicating lower switching voltages during URC and providing a way to visualize the facilitated switching in URC measurements.

In addition, in **Figure 3f,g**, we evaluate the differences between FORC and URC results. This time without considering the effective FORC switching, but the whole polarization switched for each  $V_p$ . By looking at the train sequences in **Figure 3a**, for each  $V_p$ , the integral of the charge over time in the FORC should always be larger than (or equal to) the URC case. However, as highlighted in yellow in **Figure 3d,e**, close to the coercive voltage, domains are switched faster with URC pulsing rather than with FORC pulse trains. This is true for all sweep rates, voltage resolutions, and S/NS cases. For completeness, in the Supporting information, the same analysis shown in **Figure 3** is presented for the case  $SR_H = 44 \text{ kV s}^{-1}$  (**Figure S2**, Supporting Information). In this case,  $\Delta P$  represents the difference in the integrated charge on a FORC pulse (i.e.,  $P^F(V_{p,j})$ ) and the integrated charge on the URC pulse (i.e.,  $P^U(V_{p,j})$ ) at the same voltage value  $V_{p,j}$ :

$$\Delta P = P^F(V_{p,j}) - P^U(V_{p,j}) \quad (3)$$

Interestingly, a negative value of  $\Delta P$  as seen around the coercive voltage ( $\pm 1.6 \text{ V}$ , see **Figure 3f,e**) indicating an earlier switching in URC with respect to FORC. This further confirms that the pulse train used in URC measurement has a strong impact

on the switching dynamics, namely that switching appears to be facilitated through previous partial switching. This is consistent with fluid imprint effects seen with short delay times between set and measurement pulses, whereby upon partial switching into a given polarization state, the film develops a gradual preference for that polarization state.<sup>[9]</sup>

## 2.2. Time-Dependent Imprint

To investigate the time-dependent imprint, we included delay times between voltage pulses within URC measurements, as depicted in **Figure 4**. Specifically, we evaluate six different delay times, namely  $D_1 = 100 \mu\text{s}$ ,  $D_2 = 500 \mu\text{s}$ ,  $D_3 = 50 \text{ ms}$ ,  $D_4 = 1 \text{ s}$ ,  $D_5 = 5 \text{ s}$ , and  $D_6 = 10 \text{ s}$ , obtaining the so-called Delayed-URC (D-URC) measurements. These measurements therefore represent the interplay between the fluid and time-dependent imprint on multi-level polarization switching, namely the overall imprint effect that arises when the device is left in a partially switched state for a given amount of time defined by the delay time  $D_i$ . To provide a more comprehensive visualization of the differences in terms of switching response related to different measurement techniques (i.e., URC, FORC, and D-URC), in **Figure 5** we show key cases of current density ( $J$ ) versus voltage, for positive (**Figure 5a–e**) and negative (**Figure 5f–j**) polarity. Here, thanks to the vertical lines that serve as guides to the eye, it is possible to notice that the  $V_C$  shift toward higher voltages (in absolute value) increases by increasing the delay times. Then, in **Figure 6** we present the same analysis performed in **Figure 3** for FORC (F) and URC (U) measurements, including the results associated to D-URC (D) switching. In **Figure 6a,b** we can appreciate how, upon increasing the delay time between  $V_p$ s in URC pulsing, imprint effects occur. Specifically, the results of Equation (2) are plotted in **Figure 6c,d** for  $P^U(V_{p,i})$  at each different delay time  $D_i$  (i.e., from the shortest  $P^{D1}(V_{p,i})$  to the longest  $P^{D6}(V_{p,i})$  case). For shorter delay times, we see that switching is still facilitated for voltage values close to the coercive voltage, and this is verified not only for both sweep rates (see Supporting information), but also for both polarities and all resolutions. As the delay time is increased, the previously observed facilitation of switching caused by the gradual pulse train is reduced, until a crossover occurs at  $\sim 1 \text{ s}$  and D-URC measurements lead to larger switching voltages. The results of Equation (3) are plotted in **Figure 6e,f**. Highlighted in yellow, we see the region of facilitated switching, at low delay times, close to the coercive voltage  $|1.6 \text{ V}|$ . Clearly, the imprint demonstrated here acts in the opposite direction to the fluid imprint observed in Section 2.1, so that if the capacitor is left in a partially switched state for times longer than  $1 \text{ s}$ , larger electric field magnitudes are required to switch additional domains. This suggests that unswitched domains develop a preference for their actual polarization state, which is another manifestation of time-dependent imprint. Interestingly, for higher delays (i.e.,  $D_6$ ) imprint effects are even more pronounced compared to the ones emerging in FORC measurements, i.e., leaving the device in a partially switched state has a larger impact on the  $V_C$  of unswitched domains than applying a pulse in the opposite direction directly before partial switching. It is also important to note that the effect of fluid imprint is overcome by that of the time-dependent imprint at the crossover point at

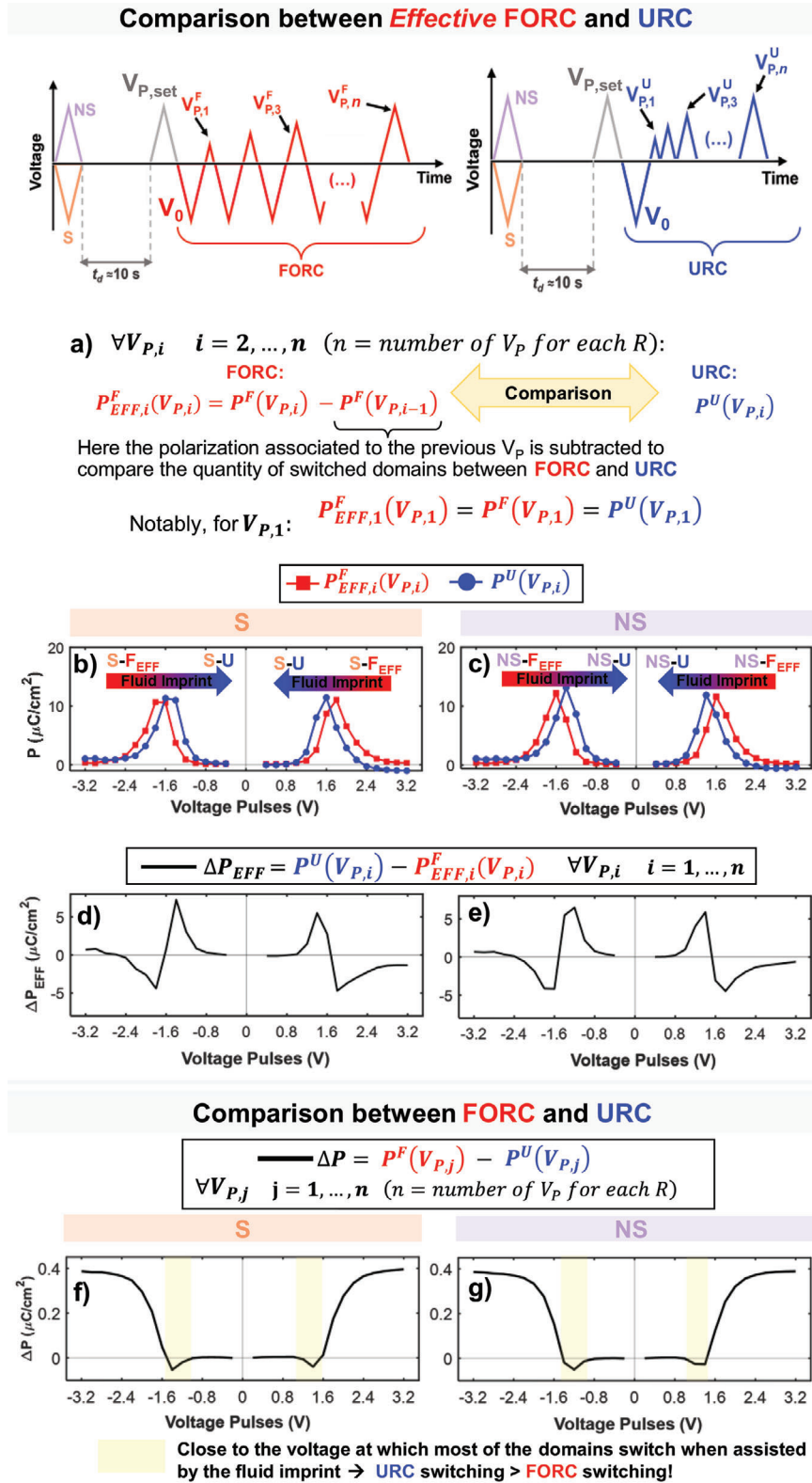


**Figure 3.** a) Pulse trains for FORC and URC measurements, and evaluation of the effective FORC polarization (i.e.,  $P_{EFF}^F$ ) for each voltage pulse. b,c) Evaluation of the differences in polarization versus voltage between effective FORC and URC measurements for the resolution  $VR_H = 0.2$  V. d,e) Differences between URC and effective FORC measurement result, presented in (b) and (c), reported for each voltage pulse. f,g) Evaluation of the differences in polarization versus voltage between FORC and URC measurements in a pulse-by-pulse manner (i.e., not considering the effective FORC polarization). All cases refer to the high-resolution  $VR_H = 0.2$  V and a sweep rate SR of  $12.6 \text{ kV s}^{-1}$ .

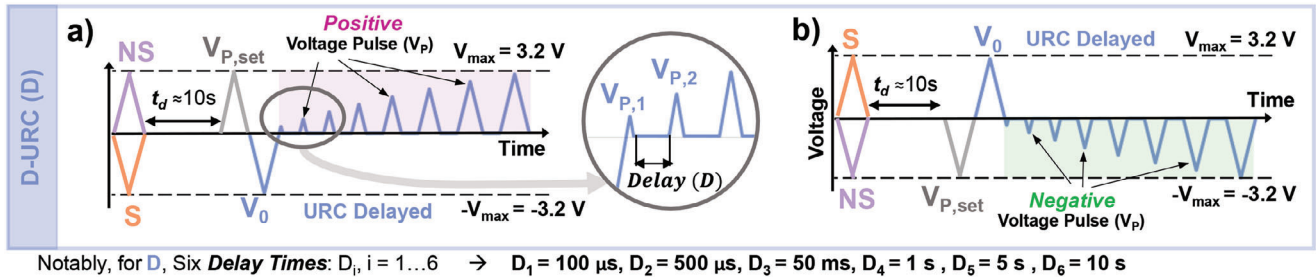


**Figure 4.** Representation of Delayed-URC (D-URC) in the case of a) positive and b) negative applied bias at the top electrode. Voltage pulses are interleaved with uniform 0 V delay times. Experiments are performed using six different delay times, ranging from 100  $\mu$ s up to 10 s.

$\sim 1$  s, while time-dependent imprint continues to act indefinitely on the ferroelectric state. This is in good agreement with the fact that the physical mechanisms behind fluid and time-dependent imprints must have different time constants.<sup>[22]</sup> For completeness, in the Supporting information, the same analysis of Figure 6 is presented for the case  $SR_H = 44$  kV s<sup>-1</sup> (Figure S3, Supporting Information).

### 2.3. A Unified Interpretation of Imprint Phenomena

Based on the outcomes of the experiments demonstrated above, in this section we propose a unified physical interpretation of imprint phenomena occurring in Hf<sub>0.5</sub>Zr<sub>0.5</sub>O<sub>2</sub>-based FeCAPs. In this interpretation, both fluid and time-dependent imprint effects are considered to be caused by charge injection from

the electrode to the non-ferroelectric layers formed at the electrode/ferroelectric interface.<sup>[34]</sup> This assumption is in line with what has been reported in literature, where fluid imprint has been attributed to electron injection into the non-ferroelectric interfacial layer due to the interface potential barrier decreasing during the applied voltage, and subsequent charge trapping at this interface.<sup>[9]</sup> Such injection is through Schottky emission or direct tunneling into the first trap state during pulse application.<sup>[18]</sup> The time-dependent imprint, instead, is associated with the subsequent charge migration across the ferroelectric bulk via Trap-Assisted tunneling (TAT) and charge trapping at defect sites mostly located both at the non-ferroelectric interfacial layers or grain boundaries within the ferroelectric bulk.<sup>[22]</sup>

In Figure 7a, we replicate the polarization versus voltage pulse plot for all three measurements types, and a sketch of the positive polarity of this plot is reported in Figure 7b. As discussed

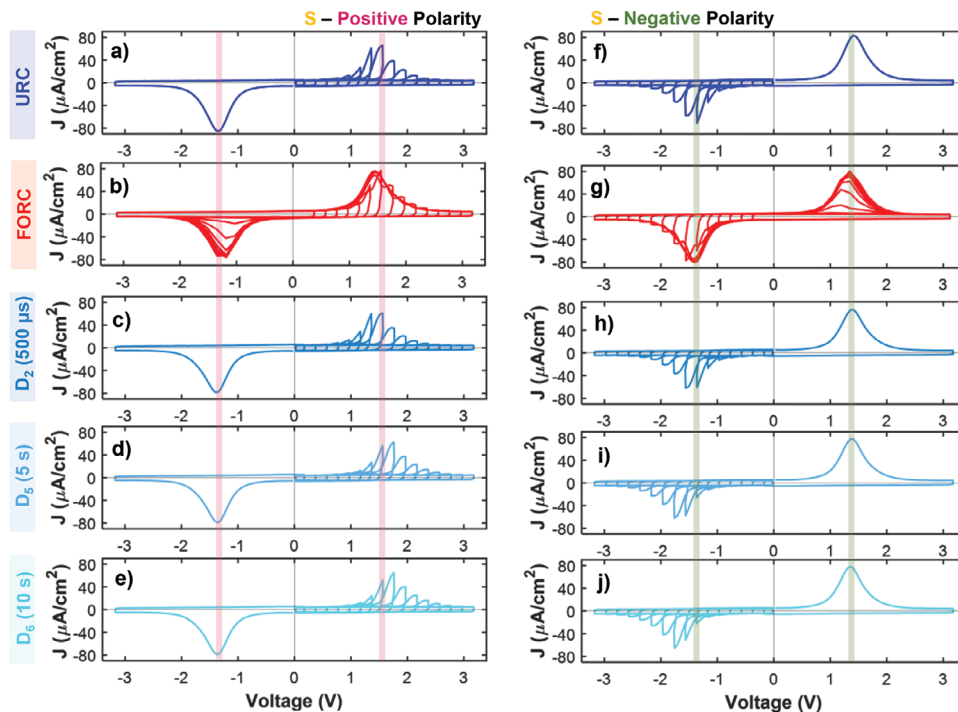


**Figure 5.** Current density ( $J$ ) versus Voltage plots for S-case measurements for positive (a–e) and negative (f–e) polarities. By increasing the delay time in between URC pulses, namely from  $D_2$  (c,h) to  $D_6$  (e,i), it is possible to notice a shift to higher coercive voltage values (in absolute value). All cases refer to  $VR_H = 0.2$  V.

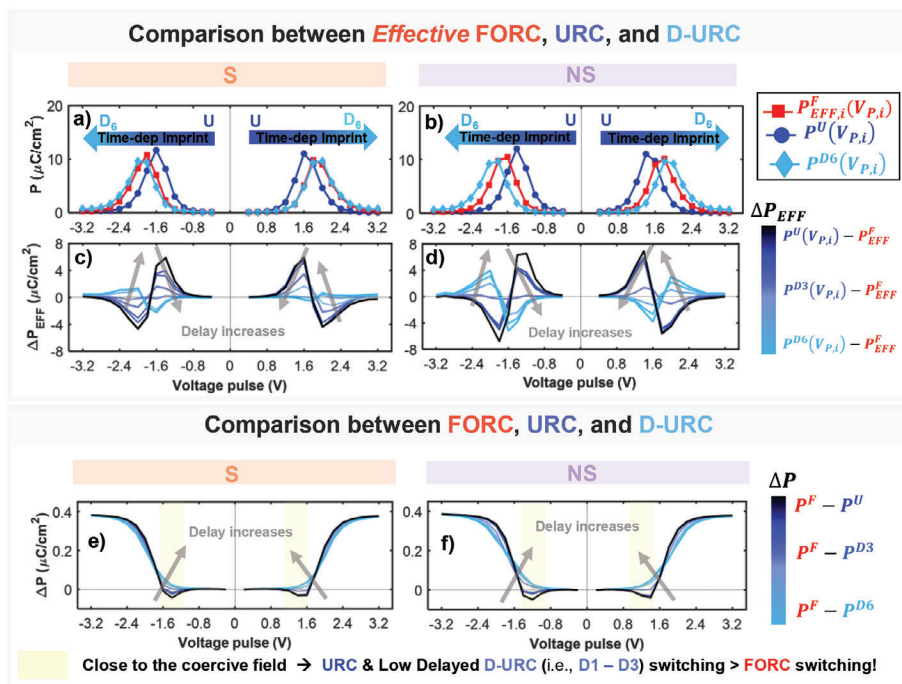


**Figure 6.** Evaluation of the differences in ferroelectric switching between effective FORC (F), URC (U), and D-URC ( $D_6$ ) for S (a) and NS (b) cases, considering the resolution  $VR_H = 0.2$  V and sweep rate  $SR_L = 12.6$  kV  $s^{-1}$ . The differences  $P_{EFF}^F - P^U$  and  $P_{EFF}^F - P^D$  (for all  $D_i$  values, namely from  $D_1 = 500$   $\mu$ s to  $D_6 = 10$  s) are reported for each voltage pulse, for the S (c) and NS (d) case. e, f) Evaluation of the differences in  $P^F$  and  $P^{U,D}$ , pulse-by-pulse.

previously (i.e., for Figure 6), in URC measurements a fluid imprint emerges, whereas upon adding a delay time between partial switching pulses ( $D_6$  in this example, i.e., 10 s) the time-dependent imprint emerges. Here, to explain the physical reasons behind our interpretation, we choose three different voltage pulses, namely A, B, and C, where  $V_{P,A} < V_{P,B} < V_{P,C}$ . Specifically,  $V_{P,A}$  may represent initial voltage pulses, e.g.,  $V_{P,1}$  and  $V_{P,2}$ , where differences in terms of switching between different measurements are less evident. In fact, as depicted in Figure 7c (Voltage Pulse A), for  $V_{P,A}$  the ferroelectric response is about the same for all the measurement types.

Differently, between Voltage Pulse A and B, it can be noted that for the URC case charges accumulated during  $V_{P,A}$  persist (as expected, since no delays are present), whereas for FORC there is a detrapping of injected charges due to the complete reversal of the polarization in the opposite orientation. Therefore, supported by the literature, the physical interpretation underlying the switching facilitation observed in URC measurement compared to FORC measurements can be associated to different charge distributions at the non-ferroelectric interfaces leading to different local internal fields.<sup>[9]</sup> For URC measurement, upon applying subsequent voltage pulses (e.g.,  $V_{P,B}$ ), additional charges are injected at the interfaces and accumulate to those already present (i.e., injected by  $V_{P,A}$ ), leading to a charge rearrangement in the layer following electrostatic repulsions. Thus, such a charge reorganization may have an impact on the local potential within the oxide reducing the electric field required for the switching of neighboring domains, or act as nuclei for further domain switching, leading to a larger number of domains switched.

Differently,  $V_{P,B}$  in FORC allows the switching of all domains characterized by switching voltages in the range  $0$  V –  $V_{P,B}$ .

The same holds for  $V_{P,C}$ , where more domains are switched with URC compared to FORC measurements thanks to the further charge rearrangement at the interface and the existence of domain nuclei, leading to a facilitated switching. Notably, for  $V_{P,C}$ , the total polarization ( $P_{TOT}$ ) switched with URC is significantly higher compared to the one switched with FORC, since the relatively steep switching curve means that even small changes to the local electric field can facilitate the switching of many domains. It should also be noted that previous experiments have shown that, at higher pulse amplitudes, more charges are injected and the detrapping time increases.<sup>[10]</sup> This offers an explanation for the behaviors highlighted in Figure 3f,g, namely, why for applied pulses close to the overall coercive voltage, partial switching in URC is facilitated in contrast to FORC where it is absent. On the other hand, the presence of delay time in between  $V_{P,s}$  characterizing D-URC measurement may allow dielectric relaxation, which has proven to occur in ALD samples,<sup>[9]</sup> and/or charge movement from the interfaces into defect traps located either at the grain boundaries within the ferroelectric bulk and/or at the opposite interface layer. Being characterized by higher time constants compared to the ones that characterize the charge electrostatic rearrangement at the interfaces (i.e., that cause fluid imprint),<sup>[22]</sup> such mechanisms occur at longer time scales, thus leading to time-dependent imprint. Notably, upon increasing the delay time, charge redistribution occurs in terms of a rearrangement in the charge configuration following trapping/detrapping events, since the diffusion of both oxygen (leading to oxygen

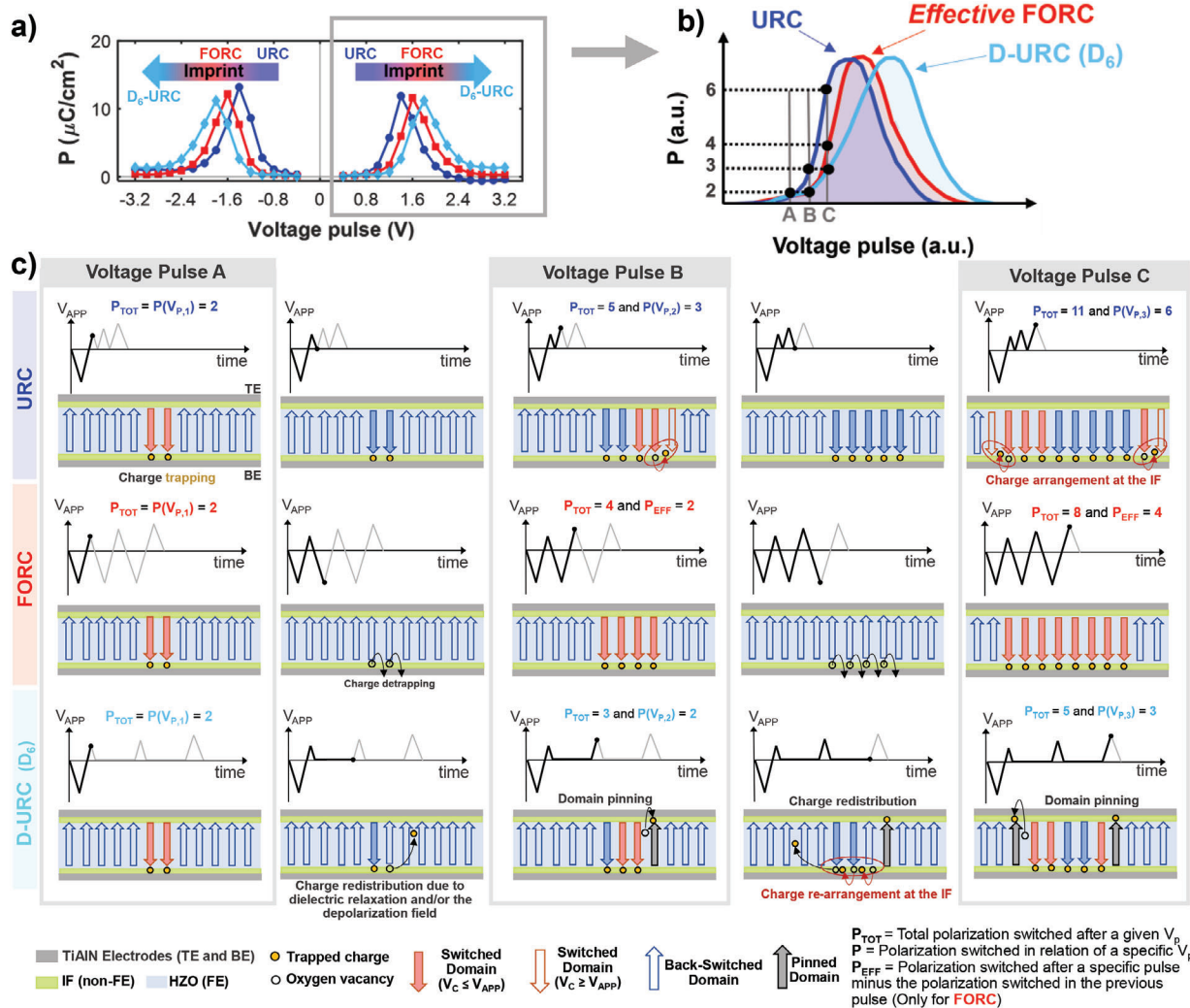


**Figure 7.** a) Evaluation of the switching characteristics between URC, FORC, and D-URC (D6) measurements, that are also reported in Figure 6a (case SR<sub>L</sub> – NS). b) Sketch of the positive side of a) in which the imprint effects are evaluated by considering three different voltage pulses, namely A, B, and C. c) Interpretation of the physical mechanisms behind both fluid (between URC and FORC measurements) and time-dependent (between URC and D-URC measurements) imprint.

vacancy movement) and other ions within the ferroelectric is unlikely at temperatures below 100 °C, due to the higher activation energy.<sup>[10]</sup> Even if evidences for field-induced migration of oxygen vacancies have been reported at room temperature,<sup>[35,36]</sup> a rearrangement in the charge configuration over time is more probable, and it provides the same consequences of defects motion in terms of local electric field perturbations. In fact, the contribution of trap-to-trap (i.e., electrons moving between traps within the oxide) tunneling was proven by simulations,<sup>[37]</sup> and such a mechanism may occur without the application of external voltage since it depends on the physical properties of the defects (i.e., thermal and relaxation energy, capture cross section). According to previous reports on HfO<sub>2</sub>-based FeCAPs,<sup>[38]</sup> the polarization switching time and the retention characteristics are well described by the Nucleation-Limited Switching (NLS) model, which attributes the polarization switching mainly to the statistics of independently nucleating domains. However, it has previously been proposed that injected charges can introduce a

temporal component to polarization switching not fully captured in NLS.<sup>[39]</sup> Interestingly, the combination of domain nucleation and time-dependent relaxation was explored via phase-field modeling to explain the accumulation of polarization on repeated voltage pulses,<sup>[40]</sup> and this delay time-dependent cumulative switching behavior has been observed in both ALD<sup>[41]</sup> and molecular beam epitaxy-deposited HZO.<sup>[42]</sup> This indicates that domain nuclei in HfO<sub>2</sub> have a finite decay time and if additional switching pulses are applied within this time, the influence of the previous pulse cannot be ignored. Conversely, when a long time delay elapses between switching pulses, classically one might expect that the pulses can be seen as isolated and the weight update would be independent of pulse history. Nonetheless, this work shows that the partially switched polarization state has a significant time-dependent influence which must be carefully considered when designing weight update schemes in ferroelectric devices. We propose that the mechanism through which the weight update is impacted by the pulse history is the injection of charges



at the interface<sup>[39]</sup> which has already been shown to impact short-term retention and imprint effects.<sup>[43,44]</sup>

As illustrated in Figure 7 for D-URC measurements, between voltage pulse A and B (as well as between B and C), charge re-configuration due to trapping processes within the ferroelectric bulk can stabilize unswitched domains through domain pinning mechanisms, which therefore require larger local fields to switch compared to unpinned domains. Remarkably, this mechanisms may explain why, for higher voltage pulses (e.g.,  $V_{P,C}$ ), fewer domains are switched compared to URC but also in comparison to FORC (explaining also the experimentally-observed crossover between FORC and D-URC at delay times of  $\sim 1$  s), thus manifesting time-dependent imprint effects. Notably, according to literature, such a pinning mechanism mainly occurs at domain seeds (seed inhibition) for HZO-based FeCAPs,<sup>[10]</sup> where seeds can be located at the interface with the electrodes or along the grain boundaries.<sup>[45]</sup>

While the results presented here were performed on devices with TiAlN electrodes, in order to prove that the impact of imprint is universal to HZO films with metallic electrodes, a standard reference TiN/HZO/TiN stack was measured, as shown in the Supplementary materials. Interestingly, an asymmetry was observed in the data on TiN electrodes, with a stronger fluid imprint in the positive polarity and time-dependent imprint in the negative polarity. Assuming the above model, it is the injecting electrode which should determine the imprint effects observed here. The top electrode in TiN/HZO/TiN, which would contribute to imprint effects in the negative polarity, is known to have a higher concentration of oxygen vacancies<sup>[46]</sup> and defects in the woken-up state,<sup>[37]</sup> which exacerbate time-dependent imprint effects.<sup>[47]</sup> Conversely, fluid imprint is seen to arise due to strong oxidation of the bottom TiN/HZO interface during ALD processing.<sup>[48]</sup> Charge injection effects also depend on the trap energies at the interfaces, as described further in the Supplementary materials. The measurements presented here can thus be used to probe asymmetries in the interfaces of ferroelectric capacitors, which have been verified experimentally and through simulations.<sup>[37,46,48]</sup>

### 3. Conclusion

In this work, a detailed analysis of imprint phenomena that typically emerge in  $\text{Hf}_{0.5}\text{Zr}_{0.5}\text{O}_2$  FeCAPs in operating conditions is presented. Thanks to the combination of FORC measurements with a new gradual switching experimental approach, named URC, both the fluid and the time-dependent imprint effects are investigated. While fluid imprint can be evaluated by means of the comparison between URC and FORC measurements, including delay times (i.e., 100  $\mu\text{s}$  – 10 s) between the voltage pulses of URC sequence not only allows us to evaluate the time-dependent imprint, but also enables the analysis of the connection between these two imprint phenomena. Finally, the experimental outcomes provided by this study, together with recent claims in the literature, allow to provide a unified physical interpretation of imprint phenomena occurring in  $\text{Hf}_{0.5}\text{Zr}_{0.5}\text{O}_2$ -based capacitors. Based on the charge injection model already presented in the literature, the interpretation proposed in this work not only elucidates the physical mechanisms underlying both fluid- and time-dependent imprint effects, but it also explains their interconnec-

tion observed in experiments. Since both phenomena can have a strong impact on multi-level polarization switching dynamics, the outcomes of this study can help to shed further light on the weight update of hafnium-based ferroelectric devices with identical or non-identical pulses. It was observed that the impact of fluid- and time-dependent imprint on multi-level switching varied in stacks with different electrodes. This suggests that routes to control these effects may be found through sample processing. For non-volatile memory applications, imprint effects should be suppressed in order to achieve repeatable multi-level switching independent (where possible) on pulse timing. However, emerging devices harnessing the synaptic function of ferroelectrics may profit from enhancing imprint effects, which act on different timescales.

### 4. Experimental Section

Capacitor stack deposition was performed as follows: 30 nm W/22 nm TiAlN (in a sandwich structure of 6 nm TiN/TiAl/6 nm TiN) was deposited on Si wafers in a high-vacuum sputter PVD tool (Alliance Concept Ct200). HZO was then deposited via ALD in 62 supercycles of  $\text{HfO}_2/\text{ZrO}_2$  (1:1) in an Oxford opAL ALD system at 280 °C. The precursors and oxidant were HyALD, ZyALD and  $\text{O}_3$ , respectively. Top electrodes of TiAlN (without W) were deposited in the same sputter tool as the bottom electrodes. Finally, capacitor structures of diameter 280  $\mu\text{m}$  were structured with Ti/Pt (5/25 nm) using a shadow mask and the top TiAlN electrode was dry etched in an inductively couple plasma tool (Oxford Instruments ICP 380) using  $\text{Cl}_2$  in order to electrically isolate the capacitors.

Electrical measurements were performed on a Cascade Microsystems probe station controlled by a Keithley 4200 SCS Parameter Analyzer. Capacitors were connected through two Keithley 4225 RPM Remote Amplifiers.

Reference samples were made by depositing TiN W/TiN (30/10 nm) in an ultra-high vacuum tool (Bestec). HZO deposition followed using the same recipe as before, and a top electrode of TiN (10 nm) was deposited before a crystallization anneal of 20 s in  $\text{N}_2$  at 600 °C. Processing followed as before but due to the lack of Al, dry etching was performed in  $\text{SF}_6$  chemistry.

Grazing-incidence x-ray diffraction (GIXRD) measurements were performed with copper X-ray source operated at 40 mA and 40 kV in a D8 Discover diffractometer from Bruker Corporation. GIXRD scans were performed with 0.2° slit placed at the incident side and a 0.2° Soller slit at the detector one. The incident angle in GIXRD was fixed to 0.45°. Indexing of the Bragg reflections was done using ab initio simulations of the lattice structures of the orthorhombic ( $o_2$ ,  $Pca_21$ ), monoclinic ( $m$ -,  $P2_1/c$ ), and tetragonal ( $t$ -,  $P4_2/nmc$ ) phases.<sup>[49]</sup>

### Supporting Information

Supporting Information is available from the Wiley Online Library or from the author.

### Acknowledgements

T.M. was financially supported out of the Saxonian State budget approved by the delegates of the Saxon State Parliament. S.L. and P.A. were financially supported through the DFG Priority Program “Memristec”, project ReLoFeMris (441909639), and through the European Commission in the Ferro4EdgeAI Project (No. GA: 101135656). R.G. was financially supported by the Deutsche Forschungs Gemeinschaft (DFG) within the project WUMM (project number: 458372836). The authors further acknowledge funding by the European Commission through the BeFerroSynaptic project (No. GA:871737) and FIXIT (No. GA: 101135398). Views and opinions expressed are those of the authors only and do not necessarily reflect those of the European Union.

## Conflict of Interest

The authors declare no conflict of interest.

## Data Availability Statement

The data that support the findings of this study are available from the corresponding author upon reasonable request.

## Keywords

charge injection, domain pinning, ferroelectric hafnia, imprint, multi-level switching

Received: March 30, 2024

Revised: May 2, 2024

Published online:

- [1] D. M. Hausmann, R. G. Gordon, *J. Cryst. Growth* **2003**, 249, 251.
- [2] T. S. Böske, J. Müller, D. Bräuhäus, U. Schröder, U. Böttger, *Appl. Phys. Lett.* **2011**, 99, 102903.
- [3] X. Tian, S. Shibayama, T. Nishimura, T. Yajima, S. Migita, A. Toriumi, *Appl. Phys. Lett.* **2018**, 112, 102902.
- [4] S. Migita, H. Ota, H. Yamada, K. Shibuya, A. Sawa, A. Toriumi, *Jpn. J. Appl. Phys.* **2018**, 57, 225.
- [5] M. H. Park, H. J. Kim, Y. J. Kim, Y. H. Lee, T. Moon, K. D. Kim, S. D. Hyun, C. S. Hwang, *Appl. Phys. Lett.* **2015**, 107, 041403.
- [6] W. Wei, X. Ma, J. Wu, F. Wang, X. Zhan, Y. Li, J. Chen, *Appl. Phys. Lett.* **2019**, 115, 2003619.
- [7] D. Zhou, J. Xu, Q. Li, Y. Guan, F. Cao, X. Dong, J. Müller, T. Schenk, U. Schröder, *Appl. Phys. Lett.* **2013**, 103, 192904.
- [8] S. S. Fields, S. W. Smith, P. J. Ryan, S. T. Jaszewski, I. A. Brummel, A. Salanova, G. Esteves, S. L. Wolfley, M. D. Henry, P. S. Davids, J. F. Ihlefeld, *ACS Appl. Mater. Interfaces* **2020**, 12, 26577.
- [9] P. Buragohain, A. Erickson, P. Kariuki, T. Mittmann, C. Richter, P. D. Lomenzo, H. Lu, T. Schenk, T. Mikolajick, U. Schroeder, A. Gruverman, *ACS Appl. Mater. Interfaces* **2019**, 11, 35115.
- [10] F. P. G. Fengler, M. Hoffmann, S. Slesazek, T. Mikolajick, U. Schroeder, *J. Appl. Phys.* **2018**, 123.
- [11] S. Mueller, J. Müller, U. Schroeder, T. Mikolajick, *IEEE Transactions on Device and Materials Reliability* **2013**, 13, 93.
- [12] M. G. Kozodaev, A. G. Chernikova, E. V. Korostylev, M. H. Park, R. R. Khakimov, C. S. Hwang, A. M. Markeev, *J. Appl. Phys.* **2019**, 125.
- [13] X. J. Lou, *J. Appl. Phys.* **2009**, 105, 024101.
- [14] Y. Higashi, B. Kaczer, A. S. Verhulst, B. J. O'Sullivan, N. Ronchi, S. R. C. McMitchell, K. Banerjee, L. D. Piazza, M. Suzuki, D. Linten, J. Van Houdt, *IEEE Trans. Electron Devices* **2020**, 67, 4911.
- [15] W. L. Warren, D. Dimos, R. M. Waser, *MRS Bull.* **1996**, 21, 40.
- [16] M. Grossmann, O. Lohse, D. Bolten, U. Boettger, R. Waser, *J. Appl. Phys.* **2002**, 92.
- [17] A. K. Tagantsev, G. Gerra, *J. Appl. Phys.* **2006**, 100, 051607.
- [18] A. K. Tagantsev, I. Stolichnov, N. Setter, J. S. Cross, *J. Appl. Phys.* **2004**, 96, 6616.
- [19] Z. Tan, J. Tian, Z. Fan, Z. Lu, L. Zhang, D. Zheng, Y. Wang, D. Chen, M. Qin, M. Zeng, X. Lu, X. Gao, J.-M. Liu, *Appl. Phys. Lett.* **2018**, 112, 152905.
- [20] J. Muller, et al. presented at 2013 IEEE Int. Electron Devices Meeting, Washington, DC, USA, December **2013**.
- [21] K. Florent, S. Lavizzari, L. Di Piazza, M. Popovici, J. Duan, G. Groeseneken, J. Van Houdt, *IEEE Trans. Electron Devices* **2017**, 64, 4091.
- [22] K. Takada, S. Takarae, K. Shimamoto, N. Fujimura, T. Yoshimura, *Adv. Electron. Mater.* **2021**, 7, 2100151.
- [23] R. Alcalá, M. Materano, P. D. Lomenzo, P. Vishnumurthy, W. Hamouda, C. Dubourdieu, A. Kersch, N. Barrett, T. Mikolajick, U. Schroeder, *Adv. Funct. Mater.* **2023**, 33, 2303261.
- [24] C. Zacharaki, P. Tsipas, S. Chaitoglou, L. Bégon-Lours, M. Halter, A. Dimoulas, *Appl. Phys. Lett.* **2020**, 117, 212905.
- [25] E. Covi, et al. presented at IEEE Int. Conf. on Flexible and Printable Sensors and Systems, Vienna, Austria, July **2022**.
- [26] S. Boyn, J. Grollier, G. Lecerf, B. Xu, N. Locatelli, S. Fusil, S. Girod, C. Carrétéro, K. Garcia, S. Xavier, J. Tomas, L. Bellaiche, M. Bibes, A. Barthélémy, S. Saïghi, V. Garcia, *Nat. Commun.* **2017**, 8, 14736.
- [27] D. Kuzum, S. Yu, H. S. Philip Wong, *Nanotechnology* **2013**, 24, 382001.
- [28] D. Ielmini, S. Ambrogio, *Nanotechnology* **2020**, 31, 092001.
- [29] M. Halter, L. Bégon-Lours, M. Sousa, Y. Popoff, U. Drechsler, V. Bragaglia, B. J. Offrein, *Commun. Mater.* **2023**, 4, 14.
- [30] S. Lancaster, et al. presented at Device Research Conf. – Conf. Digest, June **2023**.
- [31] A. Stancu, D. Ricinchi, L. Mitoseriu, P. Postolache, M. Okuyama, *Appl. Phys. Lett.* **2003**, 83, 3767.
- [32] T. Schenk, U. Schroeder, M. Pesic, M. Popovici, Y. V. Pershin, T. Mikolajick, *ACS Appl. Mater. Interfaces* **2014**, 6, 19744.
- [33] R. Alcalá, et al. presented at Technical Digest – Int. Electron Devices Meeting, December **2022**.
- [34] M. Pesic, F. P. G. Fengler, L. Larcher, A. Padovani, T. Schenk, E. D. Grimley, X. Sang, J. M. LeBeau, S. Slesazek, U. Schroeder, T. Mikolajick, *Adv. Funct. Mater.* **2016**, 26, 4601.
- [35] W. Hamouda, F. Mehmood, T. Mikolajick, U. Schroeder, T. O. Mentès, A. Locatelli, N. Barrett, *Appl. Phys. Lett.* **2022**, 120, 202902.
- [36] F. P. G. Fengler, R. Nigon, P. Muralt, E. D. Grimley, X. Sang, V. Sessi, R. Hentschel, J. M. LeBeau, T. Mikolajick, U. Schroeder, *Adv. Electron. Mater.* **2018**, 4, 1700547.
- [37] L. Benatti, S. Vecchi, M. Pesic, F. M. Puglisi, presented at IEEE Int. Reliability Physics Symp, Monterey, CA, USA, March **2023**.
- [38] N. Gong, X. Sun, H. Jiang, K. S. Chang-Liao, Q. Xia, T. P. Ma, *Appl. Phys. Lett.* **2018**, 112, 262903.
- [39] E. Kondratyuk, V. Mikheev, A. Chouprik, *ACS Appl. Electron. Mater.* **2022**, 4, 3567.
- [40] A. K. Saha, K. Ni, S. Dutta, S. Datta, S. Gupta, *Appl. Phys. Lett.* **2019**, 114, 202903.
- [41] S. Lancaster, T. Mikolajick, S. Slesazek, *Appl. Phys. Lett.* **2022**, 120.
- [42] N. Siannas, C. Zacharaki, P. Tsipas, D. J. Kim, W. Hamouda, C. Istrate, L. Pintelie, M. Schmidbauer, C. Dubourdieu, A. Dimoulas, *Adv. Funct. Mater.* **2023**, 34, 2311767.
- [43] J. Barbot, R. Fontanini, M. Segatto, J. Coignus, F. Triozon, C. Carabasse, M. Bedjaoui, F. Andrieu, D. Esseni, L. Grenouillet, *J. Appl. Phys.* **2023**, 134.
- [44] S. Lancaster, P. D. Lomenzo, M. Engl, B. Xu, T. Mikolajick, U. Schroeder, S. Slesazek, *Front. Nanotechnol.* **2022**, 4, 939822.
- [45] E. D. Grimley, T. Schenk, T. Mikolajick, U. Schroeder, J. M. LeBeau, *Adv. Mater. Interfaces* **2018**, 5, 1701258.
- [46] W. Hamouda, A. Pancotti, C. Lubin, L. Tortech, C. Richter, T. Mikolajick, U. Schroeder, N. Barrett, *J. Appl. Phys.* **2020**, 127, 064105.
- [47] K. Bao, J. Liao, F. Yan, S. Jia, B. Zeng, Q. Yang, M. Liao, Y. Zhou, *ACS Appl. Electron. Mater.* **2023**, 5, 4615.
- [48] H. A. Hsain, Y. Lee, S. Lancaster, M. Materano, R. Alcalá, B. Xu, T. Mikolajick, U. Schroeder, G. N. Parsons, J. L. Jones, *ACS Appl. Mater. Interfaces* **2022**, 14, 42232.
- [49] A. Kersch, R. Ganser, M. Trien, *Front. Nanotechnol.* **2022**, 4, 064105.